# Joint Density of States of Wide-Band-Gap Materials by Electron Energy Loss Spectroscopy

by

X.D. Fan, J.L. Peng, and L.A. Bursill

School of Physics, University of Melbourne,
Parkville, 3052, Vic., Australia

Abstract

Kramers-Kronig analysis for parallel electron energy loss spectroscopy (PEELS) data is developed as a software package. When used with a JEOL 4000EX high-resolution transmission electron microscope (HRTEM) operating at 100keV this allows us to obtain the dielectric function of relatively wide band gap materials with an energy resolution of approx 1.4 eV. The imaginary part of the dielectric function allows the magnitude of the band gap to be determined as well as the joint-density-of-states function. Routines for obtaining three variations of the joint-density of states function, which may be used to predict the optical and dielectric response for angle-resolved or angle-integration scattering geometries are also described. Applications are presented for diamond, aluminum nitride (AlN), quartz ($SiO_2$) and sapphire ($Al_2O_3$. The results are compared with values of the band gap and density of states results for these materials obtained with other techniques.

## 1. Introduction

Kramers-Kronig analysis of PEELS data is desirable in order to obtain the real and imaginary parts of the dielectric function, as well as the optical absorption coefficient and "effective electron numbers"[1-3]. These should be comparable with theoretical predictions and/or measurements made using various optical spectroscopies[3,4]. Kramers-Kronig analysis (KKA) enables the energy dependence of the real ($\epsilon_1$) and imaginary ($\epsilon_2$) parts of the permittivity to be calculated from the energy loss function, according to the method of Johnson[5-7]. There exists the possibility of obtaining additional information which may be helpful in measuring the band gap and detecting the presence of interband transitions using appropriate expressions for the joint-density-of states (JDOS) function[4]. Our commercially supplied Gatan PEELS analysis software did not perform this analysis. This paper describes the development in our laboratory of software suitable for Macintosh personal computers.

Care was taken with deconvolution of the zero-loss peak and multiple scattering events, in order to first obtain the single scattering loss function. The analysis for the dielectric function was then performed according to standard methods[1-4], using sinusoidal Fourier transforms and an inverse cosinusoidal F.T. as suggested by Johnson[5-7]. The KKA analysis was written in C using the Macintosh Programming Workshop (MPW). It is thus inserted as a Custom Function in the GATAN EL/P program. In addition we have added routines for obtaining three variations of the joint-density of states function, which may be used to predict optical and dielectric response for angle-resolved or angle-integrated scattering geometries.

Examples of applications are presented for diamond, aluminium nitride (AlN), quartz and sapphire. Although the resolution of our energy loss spectrometer is limited to 1.4 eV, the results are nevertheless interesting for relatively wide-gap materials of current and future interest. Furthermore, we may combine high spatial resolution HRTEM results, which allow nanoscale structural textures to be characterized, with the PEELS/KKA analysis of the low-loss and core-loss spectra, which provides useful information concerning the nature of the chemical bonding and mass density, as well as the dielectric response.

## 2. Theory

### (a) Single Scattering Distribution

Although the principles for this technique were developed some 25 years ago[1], they may not be familiar to current users of PEELS techniques. Probably, this situation is due to the relatively low energy resolution of the spectrometers in use with HRTEM instruments (say 0.5 - 1.5 eV). This is certainly a major limitation for most materials; however, we propose that there is a valid range of applications for materials scientists which concerns current interests in relatively wide-gap materials (say 3 eV and above, which includes blue-light emmitters and other laser materials operating in the ultra-violet). A brief statement of the principles of the method follows, the interested reader may consult Refs.[1-4] for more complete treatments of some aspects.

The relation between the scattering vector ($\mathbf{q}$) and the frequency ($\omega$) dependent dielectric function $\epsilon(\mathbf{q},\omega)$ and the electron-scattering power in an infinite medium was given by Ritchie[8].

A point charge moving with velocity $\mathbf{v}$ is represented as $-e\delta(\mathbf{r}-\mathbf{v}t)$. In an electrostatic potential $\phi(\mathbf{r},t)$, the charge satisfies Poisson's equation

$$\epsilon_0\epsilon(\mathbf{q},\omega)\nabla^2\phi(\mathbf{r},t) = e\delta(\mathbf{r},t) \tag{1}$$

For a charge moving in the $z$ direction, it can be shown using Fourier methods that the stopping power $(\mathrm{d}E/\mathrm{d}z)$ is

$$\frac{\mathrm{d}E}{\mathrm{d}z} = \frac{2\hbar^2}{\pi a_0 m_0 v^2}\iint \frac{q_y\omega \mathrm{Im}[-1/\epsilon(\mathbf{q},\omega)]}{q_y^2+(\hbar\omega/v)^2}\mathrm{d}q_y\mathrm{d}\omega \tag{2}$$

where $a_0$ is Bohr radius and $m_0$ is the electron mass. $q_y$ is the scattering vector perpendicular to the electron velocity $\mathbf{v}$ and $\omega = E/\hbar$. The stopping power can also be related to the second differential cross section (per atom) for inelastic scattering by

$$\frac{\mathrm{d}E}{\mathrm{d}z} = \iint n_a E\frac{\mathrm{d}^2\sigma}{\mathrm{d}\Omega\mathrm{d}E}\mathrm{d}\Omega\mathrm{d}E \tag{3}$$

where $n_a$ is the number of atoms per unit volume. Since $q_y = k_0\sin\theta$ and $\mathrm{d}\Omega = 2\pi\sin\theta\mathrm{d}\theta$, combining (2) and (3) gives

$$\frac{\mathrm{d}^2\sigma}{\mathrm{d}\Omega\mathrm{d}E} = \frac{\mathrm{Im}[-1/\epsilon(\mathbf{q},E)]}{\pi^2 a_0 m_0 v^2 n_a}\left(\frac{\cos\theta}{\sin^2\theta+\theta_E^2}\right) \tag{4}$$

where $\theta_E = E/(\gamma m_0 v^2)$ is the characteristic scattering angle for energy loss $E$ and $\gamma$ is the relativistic factor. In the small angle approximation, $\cos\theta \simeq 1$ and $\sin\theta \simeq \theta$ so that we obtain a Lorentzian angular factor $1/(\theta^2+\theta_E^2)$ in the differential cross-section Eq.(4). For small $\mathbf{q}$, $\epsilon(\mathbf{q},E)$ varies very slowly with $\mathbf{q}$, so that it can be replaced by $\epsilon(0,E)$ or simply $\epsilon(E)$, which can, in principle, be directly compared with the results of optical measurements.

Integrating over the scattering angle up to the experimental collection semi-angle $\beta$ and using $\mathrm{d}\Omega = 2\pi\sin\theta\mathrm{d}\theta$, the single-scattering distribution (SSD) is related to the complex permittivity or the dielectric function $\epsilon$ as

$$\begin{aligned} S(E) &= I_0 t n_a \frac{\mathrm{d}\sigma}{\mathrm{d}E} \\ &= \frac{I_0 t\ \mathrm{Im}[-1/\epsilon(E)]}{\pi a_0 m_0 v^2}\ln\left[1+\frac{\sin^2\beta}{\theta_E^2}\right] \end{aligned} \tag{5}$$

where $I_0$ is the zero loss intensity, $t$ the specimen thickness, $v$ is the electron beam velocity, $\beta$ is the collection semi-angle and $\theta_E = E/(\gamma m_0 v^2)$ is the characteristic scattering angle for energy loss $E$. $\gamma$ is the relativistic factor, $a_0$ is Bohr radius and $m_0$ is the electron mass.

### (b) Surface loss removal

Surface effects amount to some percent of the total loss probability when the specimen thickness is in its optimal range of slightly less than one mean free path for ineleastic scattering. This is of the order of 100 nm for 200 keV beam energy.

Assuming a flat and clean (unoxidized) surface and using a free electron plasmon model of the surface loss, a scattering angle of $\beta$ (with $\epsilon_a = 1$ for vacuum and $\epsilon_b = \epsilon = \epsilon_1 + i\epsilon_2$ for a specimen of thickness t) gives the single-scattering surface-loss intensity as

$$S_s(E) = I_0/\pi a_0 k_0 t[tan^{-}1(\beta/\theta_E)/\theta_E - \beta/(\beta^2 + \theta_E^2)][4\epsilon_2/((\epsilon_1 + 1)^2 + \epsilon_2^2) - \mathrm{Im}(-1/\epsilon)] \quad (6)$$

$S_s$(E) is subtracted from the experimental single-scattering distribution SSD(E) and a new normalization constant K found. Then $\epsilon$(E) is recalculated and the whole process repeated if necessary until the result converges[9]. At each stage in the procedure, the value of $\epsilon_1$ at small E (approx. equal to 2 eV) should approximate to the optical value. Egerton[3] has given a FORTRAN source code including all the necessary steps for the removal of surface effects from the single scattering distribution. This was converted to C source code and inset into our KKA custom function.

### (c) Principles of Kramers-Kronig Analysis

Based on the fact that the dielectric function is causal, it can be shown that there is a relation between the real and imaginary parts, known as the Kramers-Kronig transformation:

$$\mathrm{Re}\left[\frac{1}{\epsilon(E)}\right] = 1 - \frac{1}{\pi} P \int_0^\infty \mathrm{Im}\left[\frac{-1}{\epsilon(E')}\right] \frac{E' dE'}{E'^2 - E^2} \quad (7)$$

where $P$ is the Cauchy principal part of the integral (see e.g. Johnson[5]).

The above transformation is known as the integration method, since the whole range of Im[-1/$\epsilon(E')$] is integrated for each point of Re[1/$\epsilon(E)$]. It is, therefore, a time consuming algorithm from the computational point of view. Johnson[5-7] introduced an equivalent Fourier transform method. Considering the time-dependent dielectric function $1/\epsilon(t) - \delta(t)$, the cosine and sine transforms of its even and odd parts, $p(t)$ and $q(t)$, give Re$[1/\epsilon(E)]-1$ and Im$[1/\epsilon(E)]$ respectively. Because $1/\epsilon(t) - \delta(t)$ is a causal function, it is zero when $t < 0$ and therefore $p(t)$ is simply related to $q(t)$ as $p(t) = \mathrm{sgn}[q(t)]$.

Thus, rather than using the integration method, we may first take the direct sine transformation of Im$[1/\epsilon(E)]$ to get $q(t)$ and then apply the inverse cosine transformation of $p(t)$ to obtain Re$[\epsilon(E)]$; thus we have the real and imaginary parts of the permittivity.

Unless the specimen thickness is known exactly, we need to determinë the proportionality constant in Eq.(6). Applying the Kramers-Kronig sum rule at $E = 0$ we obtain

$$1 - \mathrm{Re}\left[\frac{1}{\epsilon(0)}\right] = \frac{2}{\pi} P \int_0^\infty \mathrm{Im}\left[\frac{-1}{\epsilon(E)}\right] \frac{dE}{E} \quad (8)$$

where $\epsilon(0) = n^2$ and $n$ is the refractive index. Alternatively, using the Bethe sum rule, we have

$$\int_0^\infty \mathrm{Im}\left[\frac{-1}{\epsilon(E)}\right] E dE = \frac{\pi}{2} E_p^2 \tag{9}$$

where $E_p$ is the volume plasmon energy loss peak position, given by

$$E_p^2 = ne^2/m\epsilon_o \tag{10}$$

$n$ is the density and $m$ is the effective mass of the valence electron.

Therefore, knowing either the refractive index or the plasmon peak position, the proportionality constant $K$ can be determined in Eq.(6) as

$$K = I_0 t/\pi a_0 m_0 v^2 \tag{11}$$

Thus, as an extra result of KKA, the absolute specimen thickness may be determined, at least in principle (c.f. Egerton and Cheng[10] for alternative methods). Once the proportionality constant is known, $\mathrm{Im}[1/\epsilon(E)]$ is readily available from Eq.(6), then we can calculate $\mathrm{Re}[1/\epsilon(E)]$ by Eq.(7).

Consequently, we can derive the real and imaginary parts of the dielectric function $(\epsilon_1, \epsilon_2)$ and $\epsilon(E)$ is given by

$$\epsilon_1(E) + i\epsilon_2(E) = \frac{\mathrm{Re}[1/\epsilon(E)] + i\mathrm{Im}[-1/\epsilon(E)]}{\{\mathrm{Re}[1/\epsilon(E)]\}^2 + \{\mathrm{Im}[-1/\epsilon(E)]\}^2} \tag{12}$$

However, the KKA procedure still depends on the assumption that the scattering vector **q** is small. For large **q**, it leads to a complicated expression for $\epsilon(q, E)$[11]. The plasmon energy $E_p(q)$ is given by

$$E_p(q) = E_p + \alpha(\hbar^2/m_0)q^2 \tag{13}$$

For example in the case of aluminium, $\alpha = 0.38 \pm 0.02$[12] and for an incident energy of 100kev and collection angle $\beta = 100$mrad, the maximum plasmon peak shift is about 0.8ev.

**(d) Band-Gap Analysis**

The imaginary part of $\epsilon_2$ measures photon absorption[12]. It is a weighted integral over the dipole oscillator strength $f_{if}$ between initial and final states[13]

$$\epsilon_2(E) = \pi e^2 \hbar^2/2mE\epsilon_0(2\pi)^3 \int f_{if} \mathrm{d}S/|\nabla_k(E_f - E_i)| \tag{14}$$

where $E_f$ and $E_i$ are the energies of the final and initial states in the interband transition and the integral is over the surface in momentum space with constant energy difference $E_f$ - $E_i$. Assuming $f_{if}$ independent of energy for the transitions involved,

$$\epsilon_2(E) \propto i/E \int \mathrm{d}S/|\nabla_k(E_f - E_i)| \tag{15}$$

The integral is known as the joint-density-of states (JDOS). It can be calculated directly from the band structure.

When both the initial and final bands are parabolic (which may be a good approximation in the vicinity of high-symmetry points in the reciprocal lattice) the gradient term is

$$\nabla_k(E_f - E_i) = \mathrm{k}\hbar^2(\mathrm{m_v} + \mathrm{m_c})/\mathrm{m_v m_c} \tag{16}$$

and the surface area $\int \mathrm{dS} = 4\pi \mathrm{k}^2$. $m_v$ and $m_c$ are the effective masses in the valence and conduction bands. Neglecting prefactors,

$$JDOS \propto \sqrt{E - E_g} \tag{17}$$

where $E_g$ is the band gap energy[14]. A steep rise (or decrease) is found for transitions next to points of high symmetry in the reciprocal lattice[13]. This can be used for qualitative interpretation of optical spectra.

If $\epsilon_1$ is large for the energy range in question, these transitions will be screened in the EEL spectrum and the loss function is then proportional to ${\epsilon_2}^4$. Consideration of Eq.(15) shows that one actually measures JDOS/E in semiconductors such as silicon.

The equation

$$JDOS \propto E^2 \epsilon_2 \tag{18}$$

is used by some authors[15–17]. As Liang[18] pointed out, this is based on the ad hoc assumption that the matrix element $\mathrm{G}_{if}$ of the momentum operator between initial and final states is independent of energy. A more natural choice is to set the oscillator strength $\mathrm{f}_{if} = 2\mathrm{G}_{if}/\mathrm{mE}$ independent of frequency, which leads to Eq.(15). The JDOS thus obtained can be compared with band calculations. This was done for titanium and vanadium carbides and nitrides with good agreement between theory and experiment[19].

When recording spectra in the microscope image mode the pre-spectrometer optics performs an integration over scattering angle. This corresponds to integration over k-space for both occupied and empty bands. It can be shown that this leads to a convolution of the density of states (DOS) of both bands[20] when calculating $\epsilon$

$$\epsilon_2(E) \propto \int \rho_i(E - E')\rho_f(E')\mathrm{d}E' \tag{19}$$

For parabolic bands, this gives

$$\epsilon_2(E) \propto (E - E_g)^2/E^2 \tag{20}$$

An EELS analysis of boron nitride along these lines yielded an optical band-gap of 4 $\pm$0.5eV[20].

When comparing EELS results on JDOS with optical experiments, it must be recalled that, according to the limited momentum resolution of the incident beam and the spectrometer, neither of the two cases described above will be seen exactly. However the scattering angles are typically less than 50 mRad for 100 keV electrons.

## 4. Software Development

To develop a program as a custom function for Macintosh computers, the basic requirements are the Gatan EL/P package with EL library and the Macintosh Programming Workshop (MPW) with C or Pascal language compiler. Our source code was written in C.

Some development of the SSD software was made to improve the treatment of the zero-loss peak. We have used both the integration and the equivalent Fourier transform methods for KKA as described above. The integration method requires much longer computation time, especially for a large number of data channels. However it allows us to verify the reliability of the Fourier method. This is important because numerical methods for fast Fourier transforms may be tricky, especially when they involve the sine and cosine transforms. Both the KK and Bethe sum rules were used to determine the proportionality constant $K$. The Bethe sum rule is usually preferred as the plasmon peak energy can be easily obtained from the low energy loss data. Note that for the angular correction of Eq.(5) we have retained $\sin^2\beta$ rather than $\beta^2$, which makes it valid to high angles (avoiding the Lorentzian approximation). We note also that Eq.(5) is strictly valid only if the loss function is independent of $\theta$, which is contradicted by plasmon dispersion. However, we used a finite (but large) collection aperture when this error is effectively negligible[2].

Prior to running our KKA custom function all spectra were deconvoluted to obtain the single scattering distribution (SSD) using the Fourier-Log method [2]. The zero-loss peaks were removed by fitting a symmetric zero-loss peak to the negative-energy tail in each of the spectra. Both these processes were carried out using our SSD software, i.e. modified Gatan EL/P software (version 2.1.1). The zero-loss peak was stored as an equivalent delta function in the first channel of the SSD and the region 0 - 5 eV was replaced by a straight line. As seen later, this placed some limitations on the band gap analysis. The surface-loss correction was then applied.

The KKA analysis was then performed as follows: the proportionality constant (K) and consequently the thickness (t) were then calculated using a sum rule; thus the loss function Im(-1/$\epsilon$) could be obtained. Then the KKA transform (Eq.8) was applied to obtain Re(-1/$\epsilon$). The real and imaginary parts of the dielectric function ($\epsilon_1, \epsilon_2$) were then calculated using Eq.(11) above. For completeness, the optical absorption coefficient ($\mu$), the core-loss spectrum and the density-of-states functions JDOS = E*$\epsilon_2(E)$ from Eq.(14), JDOS*JDOS = E$^{2}$*$\epsilon_2(E)^2$ from Eq.(17) and $E^2\epsilon_2$ = E*$\sqrt{(\epsilon_2(E))}$ from Eq.(20) were also included as part of our standard output.

The modified SSD and KKA programs were compiled and the modules installed as custom functions in the EL/P folder.

## 5. Experimental

Our results were obtained using a Gatan Parallel Detection Electron spectrometer (Model 666) attached to the JEOL-4000EX electron microscope. The resolution of the spectra was determined by measuring the full width at half-maximum (FWHM) of the zero-loss peak; this was typically close to 1.4eV when the JEOL-4000EX was operated at 100kv. All PEELS data referred to here were recorded at 100kV. The collection angles used were 5.25, 11.5, 17.1 and 33.1 mrad, corresponding to the four available objective apertures. Wherever possible data sets were recorded for a set of spot sizes and objective apertures. The convergence angle was typically 1 mrad. The spectra were typically measured from areas about 120nm in diameter, recording times were 120s for core loss and 0.3s for low loss spectra. Spliced segment processing was often used to piece together two segments of spectra acquired over low and higher energy-loss ranges. The HRTEM images were recorded at 400keV. Note that our JEOL 4000EX instrument has been successfully configured to allow rapid switching of the instrument alignments between 400 keV and 100 keV operation.

HRTEM images and PEELS spectra from a variety of wide-gap materials were acquired under identical condition; referred to in this paper are crystalline diamond obtained by chemical-vapour-deposition, aluminum nitride, grown by reactive magnetron sputtering, high purity synthetic quartz and pure sapphire substrate material obtained commercially.

Thin specimens suitable for electron microscopy were prepared by simply placing clean, dry freshly crushed powders onto 1000 mesh copper grids. This technique significantly reduces electron beam irradiation damage and chemical contamination of the specimens during observation.

HRTEM was used to select areas which appeared relatively homogeneous and of slowing increasing thickness. Images were recorded using a JEOL-4000EX electron microscope operating at 400keV; the spherical aberration coefficient of the ultra-high resolution pole-pieces was Cs=0.94mm and the effective Scherzer or interpretable image resolution is 0.17nm. The specimen height was carefully adjusted to an optimum focusing current, when the objective lens astigmatism as well as the optical alignment parameters could be set precisely against calibrated values.

The PEELS data were recorded at 100 keV, the data were rejected if there was apparent microstructual damage or specimen contamination over the area being illuminated by the electron beam; this was monitored by comparing images before and after recording the electron energy loss spectra. Note that lens current and alignment settings were stored in memory so that it was a relatively straightforward matter to switch between 400 and 100 keV operation.

## 6. Results

Fig. 1 shows the loss functions Im(-1/$\epsilon$) for quartz, sapphire, aluminum nitride and diamond respectively. Note the relatively sharp onset at approx. 10 eV for quartz and 8 eV for sapphire, which are consistent with the published band gap calculations of 8.9 eV and 7.14 eV for quartz and sapphire respectively. Such a correspondance is not so clear for AlN

and diamond, which we expect have band gaps of 6.2 eV and 5.5 eV respectively. This is because of our use of a linear fit to the single-scattering distribution applied to the first 5 eV of the data. Nevertheless, the loss function onset is clearly consistent with those values for the band gap.

Fig. 2 gives the results for JDOS for quartz, sapphire, aluminium nitride and CVD diamond respectively. The results for diamond and AlN are as expected for the available energy resolution (1.4 eV at 100 keV), with information about the band gaps (5.5 and 6.2 eV respectively) being lost in the range 0 - 5 eV. However, for sapphire and quartz we can locate the band gaps reliably at 8 eV and 9 eV respectively. Despite these experimental limitations we have obtained useful representations of the JDOS function in all four cases.

Fig. 3 shows the results for JDOD*JDOS for quartz and sapphire respectively. According to Eq.(16) above, which assumed parabolic bands, one should obtain the band gap $E_g$ from the intercept of the leading edge on the energy axis of this plot. Doing this yielded values for $E_g$ of 9 eV and 7.8 eV for quartz and sapphire respectively (c.f. predicted values of 8.9 eV and 7.14 eV respectively). Due to the limitations of the SSD in the range 0 - 5 eV we did not attempt such an extrapolation for AlN and diamond.

Fig. 4 shows the corresponding results for $E^2\epsilon_2(E)$ for quartz and sapphire respectively. According to Eq.(19) above, which also assumed parabolic bands as well as angle-integrated data, one should obtain the band gap $E_g$ from the intercept of the leading edge on the energy axis of this plot. In this case there was no straight line portion to extrapolate.

## 7. Discussion

Despite the limited resolution (apprx. 1.4 eV) of our energy-loss spectrometer and our use of a linear fit for 0 - 5 eV for the SSD we have been able to obtain good results for the band gaps of quartz and sapphire. These are wide-gap materials in common use as substrates in modern electronic and optical technologies. Figure 5 shows the density of states and energy band structure calculated for sapphire[21]. Ideally, one would aim to use such results to predict the joint-density-of-states function JDOS for comparison with the above results. Note that in our experiments we are limited effectively to the zero wavevector limit (i.e. the $\Gamma$ point). Thus we expect to obtain only the direct energy gap.

Of course the electron energy loss techniques used above have lower resolution than optical methods. However, they do have some advantages. Firstly, they covers a wider energy range which may include the ranges covered by visible, ultraviolet and soft x-ray radiation. Second, in combination with high resolution electron microscopy, it allows the structure of localized regions to be characterized, along with their PEELS spectra[22]. The low energy resolution gives rise to difficulties near the zero-loss region, over 0 - 5 eV in fact for our instrument. Therefore, at this stage, the KKA method can only reliably measure wide band-gaps for insulating materials like sapphire and quartz. We expect that this limitation can be overcome by increasing the instrumental resolution as well as being extremely careful with the zero-loss peak simulation to obtain more accurate single scattering distributions in the range 0 - 5 eV. We are currently attempting to implement the above KKA procedures using data obtained using VG-STEM nanoprobe instruments which have energy resolution of 0.5 eV, when we

expect to obtain useful results for diamond, aluminium nitride and other interesting wide-gap semiconductors, insulators and glasses.

## Acknowledgements

The authors wish to thank Australia Research Council for financial support of this project. X.D. Fan is grateful for the award of an ARC Postdoctoral Research Fellowship (1993-5). We thank MingShen Liu for the nitride specimen and Sue-Ann Stuart for the CVD diamond. We are also grateful to David Dryden for his support of the HRTEM/PEELS instrumentation at the University of Melbourne.

## REFERENCES


1. J. Daniels, C. von Festenberg, H. Raether and K. Zeppenfeld, *Springer Tracts in Modern Physics*, **54**, 72-135 (1970).
2. R.F.Egerton, *Electron Energy Loss Spectroscopy in the Electron Microscope*, Second Ed., New York, (1996).
3. J.Fink, *Advances in Electronic & Electron Physics*, **75**, 121-231 (1989).
4. P. Schattschneider and B. Jouffrey, *Energy-Filtering Transmission Electron Micrsocopy*, L. Reimer (Ed.), Springer-Verlag, Berlin, Ch.3, 151-224 (1995).
5. D.W. Johnson, *J. Phys. A:Maths and Gen.*,, **8**, 490-495 (1975).
6. D.W. Johnson and J.C.H. Spence, *J. Phys.*, **D7**, 771-780 (1974).
7. D.W. Johnson, PhD Thesis, University of Melbourne (1976).
8. R.H. Ritchie, *Phys. Rev.* **106**, 874-881 (1957).
9. C. Wehenkel, *J. Phys. (Paris)* **36**, 199-213 (1975).
10. R.F. Egerton and S.C. Cheng, *Ultramicros.*, **21**, 231-244 (1987) .
11. C.J. Tung and R.H. Ritchie, *Phys. Rev.*, **16**, 4302-4313, (1977).
12. K. Utsumi and S. Ichimaru, *Phys. Rev. A*, **26**, 603-610 (1982).
13. H. Ibach and H. Luth, *Solid State Physics*, Springer, Berlin (1990).
14. J.C. Phillips, *Bonds and Bands in Semiconductors*, Academic Press, New York (1973).
15. K. Zeppenfield, *Z. Physik*, **243**, 229-243 (1971).
16. G. Leveque, S. Robin-Kandare and L. Martin, *Phys. Stat. Sol.(b)*, *63*, 679-690 (1974).
17. M.D. Martin and B.L. Averbach, *J. Non.Cryst. Solids*, **12**, 391-421 (1973).
18. W.Y. Liang and A.R. Beal, *J. Phys. C*, **9**, 2823-2832 (1976).
19. J. Pfluger, J. Fink, W. Weber and K.P. Bohmen, *Phys. Rev.B*, **30**, 1155-1163 (1984).
20. W.G. Saintly, P.L. Martin, R.P. Netterfield, D.R. McKenzie and D.J.M. Cockayne, *J. Appl. Phys.*, **64**, 3980-3986 (1988).
21. R.H. French, *J. Amer. Ceram. Soc.*, **73**, 477-489 (1990).
22. J.L.Peng, X.D.Fan and L.A. Bursill, *Inter. J. Mod. Physics. B*, **10**, 3875-3892 (1996).

## FIGURE CAPTIONS

**Figure 1**
Typical loss function ($Im(-1/\epsilon)$) results for crystalline quartz, sapphire, aluminum nitride and diamond, following KKA.

**Figure 2**
Comparison of JDOS results for quartz, sapphire, AlN and diamond.

**Figure 3**
Comparison of JDOS*JDOS results for quartz and sapphire.

**Figure 4**
Comparison of $E^{2}*\epsilon_2$ results for quartz and sapphire.

**Figure 5**
Theoretical density of states results for sapphire[21]. Note direct band gap of 7.14 eV and density of states for the valence and conduction bands.

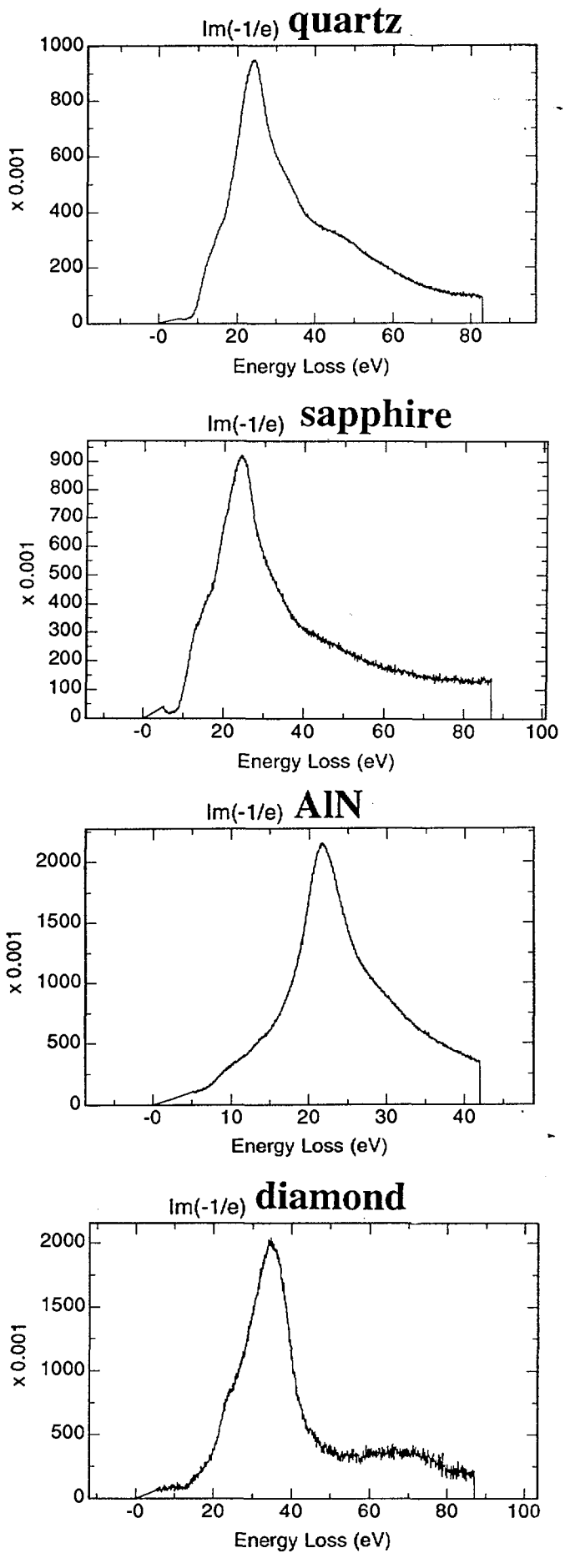
Im(-1/e) quartz
x 0.001
Energy Loss (eV)
Im(-1/e) sapphire
x 0.001
Energy Loss (eV)
Im(-1/e) AlN
x 0.001
Energy Loss (eV)
Im(-1/e) diamond
x 0.001
Energy Loss (eV)

**Figure 1**

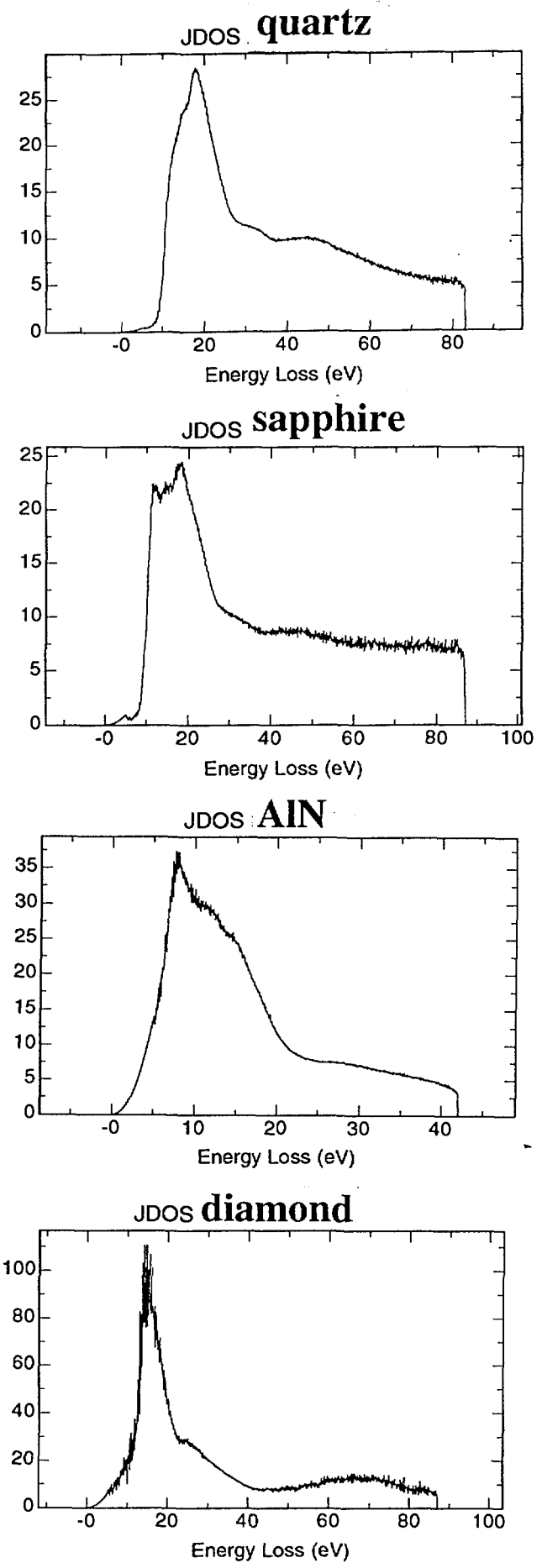
JDOS quartz
25
20
15
10
5
0
-0
20
40
60
80
Energy Loss (eV)
JDOS sapphire
25
20
15
10
5
0
-0
20
40
60
80
100
Energy Loss (eV)
JDOS AlN
35
30
25
20
15
10
5
0
-0
10
20
30
40
Energy Loss (eV)
JDOS diamond
100
80
60
40
20
0
-0
20
40
60
80
100
Energy Loss (eV)

**Figure 2**

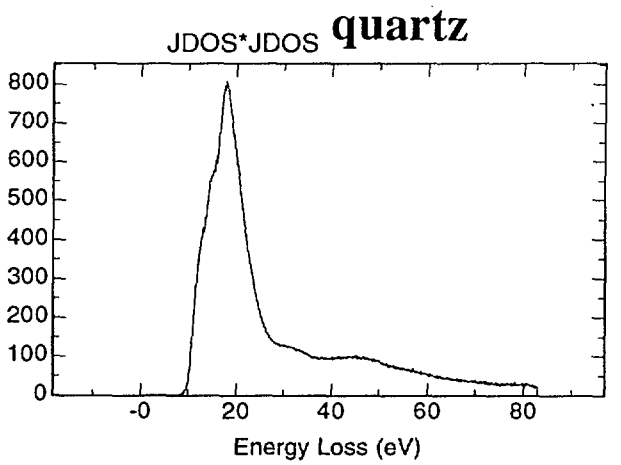
JDOS*JDOS quartz
800
700
600
500
400
300
200
100
0
-0
20
40
60
80
Energy Loss (eV)

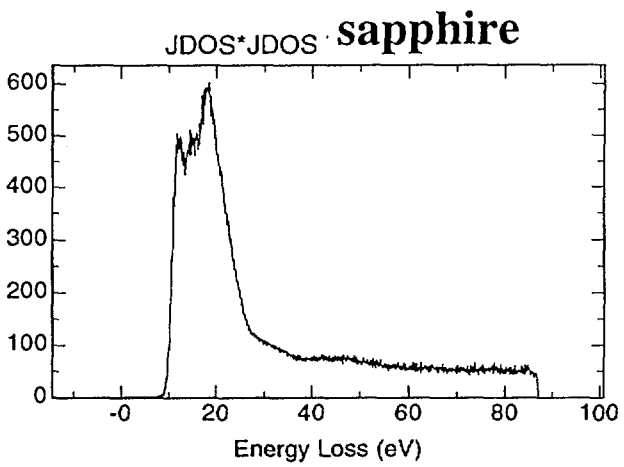
JDOS*JDOS sapphire
600
500
400
300
200
100
0
-0
20
40
60
80
100
Energy Loss (eV)

**Figure 3**

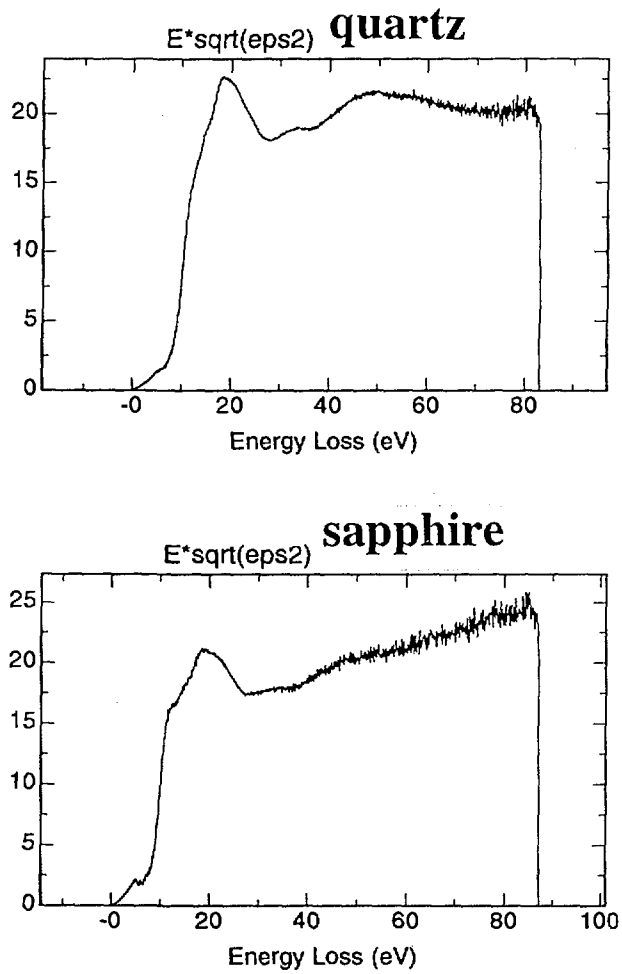
E*sqrt(eps2)
quartz
20
15
10
5
0
-0
20
40
60
80
Energy Loss (eV)
E*sqrt(eps2)
sapphire
25
20
15
10
5
0
-0
20
40
60
80
100
Energy Loss (eV)

**Figure 4**

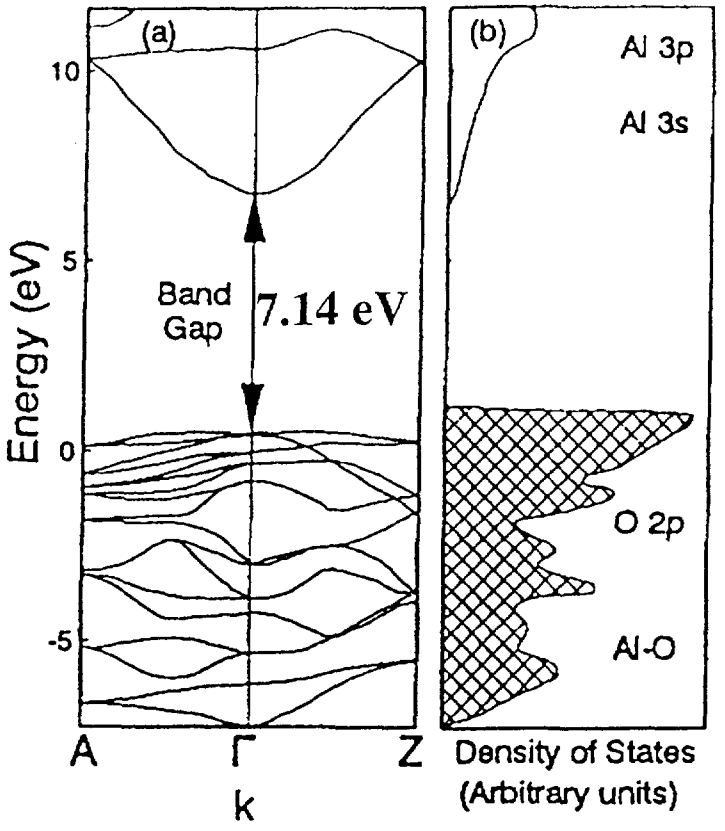
(a)
(b)
10
5
0
-5
Energy (eV)
Band Gap
7.14 eV
Al 3p
Al 3s
O 2p
Al-O
A
Γ
Z
k
Density of States
(Arbitrary units)

**Figure 5**